The Journal of Experimental Biology 211, 3563-3572
Published by The Company of Biologists 2008
doi:10.1242/jeb.018010

Flexibility foils filter function: structural limitations on suspension feeding

Matthew C. Ferner* and Brian Gaylord
Bodega Marine Laboratory and Section of Evolution and Ecology, University of California at Davis, Bodega Bay, CA 94923, USA
*Author for correspondence (e-mail: mcferner@ucdavis.edu)

Accepted 15 September 2008

SUMMARY

Suspension feeders rely on filter structures of a variety of forms to capture food particles. Much effort has been devoted to examining the operation of such filters, but mechanistic evaluations have generally represented filter elements with artificially stiff cylinders. We extended this previous work to investigate how bending affects the function of flexible cylindrical filter elements. Scaled models of filters were constructed from materials with elastic moduli comparable to material stiffnesses of invertebrate appendages (1–177 GPa). These models were mounted on a sled to mimic the protrusion of filters away from an animal's body or from the substratum, and were towed through a vat of syrup to generate relative fluid motion at low Reynolds numbers ($Re<10^{-3}$, based on cylinder diameter and tow speed). Flow between filter elements was quantified at multiple positions along their lengths, and a hydrodynamic index of filter performance ('leakiness') was calculated. Leakiness generally increased with cylinder *Re* and distance from the filter base. At higher flexibilities, however, streamwise bending and lateral narrowing of the filter reduced projected area and slowed flow between elements. This effect decreased leakiness and reversed the otherwise monotonic trend for increased leakiness at higher cylinder *Re*. Additional experiments showed that filters composed of stouter elements were less susceptible to bending but experienced lower leakiness because of their reduced ability to transcend boundary layers formed over surfaces to which they attached. These findings indicate that filter bending can strongly alter the performance of particle capture apparatus in suspension feeders.

Key words: functional morphology, structural flexibility, elastic modulus, filtration, leakiness, low Reynolds number, cylindrical arrays, biomechanics.

INTRODUCTION

Suspension feeders provide an important link in both benthic and pelagic marine food webs by capturing particulate organic matter from the water column and by serving as food themselves for many consumers (e.g. Gili and Coma, 1998). Recognizing their ecological significance, numerous researchers have examined flow effects on particle capture by these animals (e.g. Koehl and Strickler, 1981; Leonard et al., 1988; Hunter, 1989; Patterson, 1991; Lacoursière and Craig, 1993; Larsson and Jonsson, 2006) (reviewed by Wildish and Kristmanson, 1997). The traditional point of departure for understanding the mechanics of particle capture has been hydrosol filtration theory, commonly applied to idealized collector arrays composed of perfectly rigid cylinders (Rubenstein and Koehl, 1977; LaBarbera, 1984; Shimeta and Jumars, 1991). A key index emerging from this conceptualization is 'leakiness', a measure of filter efficacy quantified as the proportion of water passing through an externally held feeding array, relative to the flow impinging on it (Cheer and Koehl, 1987). Based on many studies (e.g. Hansen and Tiselius, 1992; Loudon et al., 1994; Koehl, 1995; Mead and Koehl, 2000), much is now known about how leakiness varies as a function of geometry and collector Reynolds number ($Re=Ud\rho/\mu$; a measure of the relative importance of inertial and viscous forces in a flow past a collector, where U is an appropriate velocity scale, d is the collector diameter, ρ is the density and μ is the dynamic viscosity).

Despite these advances, notable gaps remain in understanding even the most basic features of suspension feeding. One important omission has been a systematic appreciation for the consequences of deformation. The structural flexibility of appendages of real animals enables them to deflect in flow, creating deviations from the idealized case. For example, filter bending can reduce imposed forces and expand the range of flow conditions under which feeding is possible (Patterson, 1984; Harvell and LaBarbera, 1985; Sponaugle and LaBarbera, 1991). Deflection can also have negative effects because the area of a filter array facing flow is diminished by bending.

To begin to isolate the consequences of structural flexibility for filter function, we examined leakiness through simple but deformable physical models composed of multiple cylindrical elements. These artificial filters extended away from a solid surface, mimicking the situation faced by animals that hold filter arrays away from the substratum or from their own support structures. Because we wanted to distinguish effects of filter bending from other factors, we focused on relatively low cylinder *Re* ($\sim10^{-5}$ to $\sim10^{-3}$, with U set equal to the free-stream velocity outside local boundary layers adjacent to animal bodies or the seafloor). Reynolds numbers of suspension feeders extend across a much broader range ($<10^{-6}$ to >10) (Vogel, 1994), but the higher end of this range is characterized by leakiness values that depend strongly on hydrodynamic processes that interact with other factors (Koehl, 1995; Loudon and Koehl, 2000). Our results, derived for the more easily interpreted range of lower *Re* conditions, indicate clearly that the bending of feeding appendages can strongly influence filter leakiness and the capacity for particle capture. Effects of collector deflection at low *Re* may apply to a variety of suspension-feeding animals that experience flows as slow as $0.1\,mm\,s^{-1}$ and possess small filtering structures (~0.1–10 μm diameter), including flagellated protozoans, cladocerans, bryozoans and serpulid

Table 1. Summary of parameter values from studies that employed physical models composed of cylindrical elements to examine filter leakiness

Study	Elastic modulus (GPa)	Tank size (m^3)	*Re*	Number of cylinders	Gap to diameter ratio	Length to diameter ratio
Hansen and Tiselius (1992)	~160*	0.005, 0.012	0.005–40	2–12	1–80	25–108
Leonard (1992)	180*	0.38	1.7–197	3–33	0.5–15	10–40
Loudon et al. (1994)	160*	0.13	10^{-4}–1	2	2.5–30	∞ (entire depth)
Mead and Koehl (2000)	>180*	0.13	0.13–1.68	3 in each of 4 rows†	1†	26–32
Current study	1–180	0.47	10^{-5}–10^{-3}	4	5	50–100

*Estimated from known engineering properties of cylinder materials used by the author.
†Parallel rows of cylinders were spaced at distances of either 7.5 or 16 cylinder diameters.

polychaetes, among others (e.g. Turner et al., 1988; Scardino et al., 2008).

MATERIALS AND METHODS

Experimental approach

We generated fluid motion relative to model filters of suspension feeders by towing arrays of cylinders through a stationary volume of fluid, employing geometries representative of a variety of invertebrate taxa (reviewed by Cheer and Koehl, 1987; Leonard, 1992), and incorporating model materials of a range of flexibilities (Table 1). We then considered ensuing filter deformations within the following generalized framework. Taking as a starting point the simplified case of flow past a single, perfectly rigid cylinder far from a solid surface, there are five variables that influence the magnitude of force (F) imposed on the cylinder. These variables are ρ, U, μ, d and the length of the cylinder, L. This suite of parameters can be combined using techniques of dimensional analysis (e.g. Fox and MacDonald, 1985) to produce the relationship:

$$\frac{F}{\rho U^2 d^2} = f\left(\frac{\rho U d}{\mu}, \frac{L}{d}\right). \quad (1)$$

This expression states that the imposed force, once normalized for cylinder size, flow speed and fluid properties, is a function exclusively of collector *Re* and the aspect ratio of the cylinder, as is the flow field past the cylinder. A complication arises if the cylinder is affixed at one end to a smooth support surface, since velocities are slowed within the boundary layer adjacent to that surface. If the boundary layer is laminar rather than turbulent (as is typical of the very low *Re* flows that are the focus of our study), then the thickness of the boundary layer, and thus the degree to which velocities incident on the cylinder are reduced, depends exclusively on ρ, U, μ and the distance, x, of the attachment point of the cylinder from the upstream edge of the surface (Schlichting, 1979). This situation creates a positional effect defined by the parameter x/d, leading to the equality:

$$\frac{F}{\rho U^2 d^2} = f\left(\frac{\rho U d}{\mu}, \frac{L}{d}, \frac{x}{d}\right). \quad (2)$$

A final consideration arises if the cylinder is imperfectly rigid, since it then bends in response to flow by a magnitude dictated by its modulus of elasticity, E, a measure of its material stiffness. If the cylinder is always at dynamic equilibrium with the fluid such that cylinder accelerations or decelerations are negligible (this assumption is appropriate at low *Re*), then a specific force will always cause a given degree of bending in any particular cylinder. This bending can be indexed using the ratio δ/L, which quantifies the lateral deflection of the cylinder's tip (δ) relative to its length. A dimensional analysis of the bending process, coupled with Eqns 1 and 2, leads to the expression:

$$\frac{\delta}{L} = f\left(\frac{\rho U d}{\mu}, \frac{L}{d}, \frac{x}{d}\frac{E}{\rho U^2}\right). \quad (3)$$

This equality indicates that the extent of deflection of a flexible cylinder protruding perpendicularly into flow depends only on collector *Re*, the aspect ratio of the cylinder, the point of attachment of the cylinder within the boundary layer formed over the cylinder's support surface, and the parameter $E/(\rho U^2)$ (henceforth $=B$). B is the nondimensional stiffness, equal to the modulus (E) divided by twice the dynamic pressure of the flow (Fox and MacDonald, 1985).

In more complex geometries beyond solitary cylinders, including multiple cylinders in arrays, additional dimensionless parameters become important. They include the ratio of gap width between cylinders to cylinder diameter, the ratio of the width of a multiple-cylinder array to cylinder diameter, and (in the case of laboratory experiments) ratios of tank or other apparatus dimensions to cylinder diameter. In situations where cylinders protrude from rough surfaces into turbulent regions of benthic boundary layers, two further parameters arise (the ratio of roughness height to cylinder diameter, and another Reynolds number based on U^*, the so-called 'friction velocity') (Eckman and Nowell, 1984).

We focused on a subset of the full parameter space spanned by the governing variables identified above. For each of three values of collector *Re* between approximately 10^{-5} and 10^{-3}, we tested cylinder aspect ratios, L/d, of 50 and 100. Given the dimensional analysis described above, the use of Reynolds numbers based on free-stream velocities, rather than 'face velocities' incident on the filter array, simplified the approach. However, we acknowledge that this convention [also used by other researchers (e.g. Cheer and Koehl, 1987)] interferes in some circumstances with easy interpretation. Values of E have not been measured for intact suspension-feeding appendages, yet natural polymer composites that make up these structures have elastic moduli on the order of 0.1–100 GPa (Wegst and Ashby, 2004). In aquatic environments characterized by relative velocities of 10^{-4}–1 $m\,s^{-1}$, it follows that actual values of B range from approximately 10^5 to 10^{16} for most suspension feeders, but we restricted experiments to the upper end of this range to avoid a disproportionate emphasis on consequences of extreme bending. We held the parameter x/d constant in all experiments. We considered only one ratio of gap width to cylinder diameter, one ratio of array width to cylinder diameter, and single ratios of apparatus dimensions to cylinder diameter. These restrictions obviously limit our ability to generalize across the full breadth of conditions occurring in nature, so we focused on phenomena that are likely to be general across a wide choice of cylinder arrays, emphasizing qualitative results that ensued from

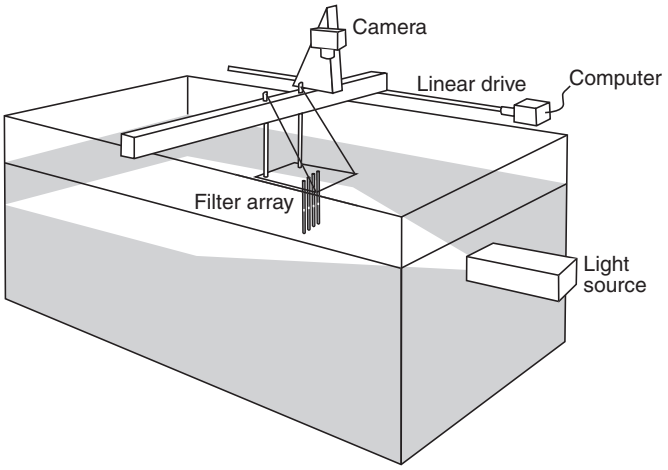

Fig. 1. Schematic of low Reynolds number tank used for visualizing flow-through model filters. An array of four cylindrical filter elements, oriented vertically, was fixed to a sled that was towed through viscous syrup using a computer-controlled linear drive. This motion produced relative flow through the model filter analogous to currents passing through feeding appendages of suspension feeders. Overhead images of flow between filter elements were collected with a camera focused on a thin light sheet projected through the end of the tank. Longest dimension of the tank measured 1.25 m, for scale.

the quantitative measures we undertook using specific filter sizes and geometries.

Low Reynolds number tank

The rectangular tank (Fig. 1) we used for experiments was filled with 416 l of high-viscosity corn syrup (ADM LSI Specialty Products, Liquidose 434, San Leandro, CA, USA). The tank was 1.25 m long, 0.57 m wide and 0.61 m high (larger than chambers used in previous studies) which reduced wall effects as much as was feasible. Although it was not possible to entirely eliminate such effects (Vogel, 1994), filter structures inherently operate in close proximity to other solid surfaces (e.g. bodies, neighbors or substratum) and our intention was to compare filter performance in the context of biologically reasonable geometries. Dynamic viscosity of the syrup was measured with a digital viscometer (Brookfield Engineering Labs, Model HBDV-E, Middleboro, MA, USA) and density was calculated by weighing a known volume. The syrup was thoroughly mixed 10 days prior to experiments so that large entrained air bubbles, which would have interfered with model visualization, had time to float to the surface and be removed. A nearly uniform suspension of small bubbles [mean (± s.d.) diameter=123 (±33) μm; N=100] remained trapped in the syrup, rising only exceptionally slowly (<2 mm day^{-1}) and thereby serving as tracer particles for flow visualization (see Filter leakiness, below).

Model filter arrays

Scale models of organism filter arrays were constructed using four parallel and vertically oriented, cylindrical rods spaced evenly in a row perpendicular to the direction of motion. Cylinders were inserted into predrilled holes in the central region of a transparent acrylic sled (230 mm long, 160 mm wide, 5 mm thick) that rested on the fluid surface. The longest axis of the sled was aligned with the direction of motion, and the leading and trailing edges of the sled were curved upward to facilitate travel across the fluid surface. Filter arrays were centered on the sled at a distance of 56 mm (~35 cylinder diameters) from the leading edge, and all cylinders had a diameter (d) of 1.59 mm. The cylinders extended either 159 or 79.5 mm into the flow (referred to as 'slender' and 'stout' arrays, respectively, where L is cylinder length). The gap between adjacent cylinder edges was 7.95 mm (5d), yielding a total array width of 30.2 mm (19d) for all filters.

Each array contained cylinders composed of one of the following materials: stainless steel (type 316), brass (alloy 260), Garolite-G10 (glass-cloth laminate plastic), Garolite-XX (paper-based laminate plastic), or nylon (6/6). Materials were selected to represent the natural range of structural flexibility found in materials composing biological fibers, hairs and setae of real animals (Wegst and Ashby, 2004). The elastic modulus (E) of each model material was measured using three-point bending tests conducted on an Instron materials testing device (Model 3345, Norwood, MA, USA).

Filter deformation

Relative fluid motion through and around the filter arrays was generated by towing the model filters through the syrup using a micro-stepping motor (Oriental Motor Company, Model RK564AA, Torrance, CA, USA) driven by motion-control software (National Instruments, NI-Motion v.1.2). Filters were towed at each of three velocities (U=0.3, 3.0, or 30 mm s^{-1}). After filter elements reached a steady state, the filters were photographed through the walls of the tank using a 35 mm camera (Nikon D70s, 60 mm lens). The spatial coordinates of each filter array (in both side and end views) were recorded under conditions of no motion and at all tow velocities, in order to determine the extent of streamwise bending of the array, lateral compression or narrowing of the array, and the resultant projected filter area as viewed from directly upstream.

Filter leakiness

Fluid motion between individual filter elements was measured by quantifying displacements of suspended tracer particles relative to the filter over time, a technique known as particle tracking velocimetry. Overhead images were collected by mounting the 35 mm camera directly above the sled and focusing it on a plane located at a known distance below the base of the filter array. Trials were run in the dark and fluid motion at the target height was illuminated with a light sheet (5–7 mm thick) produced by shining a synchronized flash (Nikon Speedlight SB-800) through a 1-mm slit at the upstream end of the tank. As before, the sled was towed at the chosen test velocity until filter elements reached steady-state deflection. Four successive images then were collected at regular intervals during each trial to allow sufficient particle displacement for velocity determination. In experiments with slender filter elements (L/d=100), images were collected at 10, 30, 50, 70, 90, 110, 130 and 150 mm from the filter base. In experiments with stout filter elements (L/d=50), images were collected at 10, 30, 50 and 70 mm from the filter base. The order of the three tow velocities was determined randomly for each light sheet position. Replicate trials (three per condition) were collected on different days and this same protocol was applied to filter arrays composed of each of the five materials examined in the study, resulting in 540 total experimental trials.

Images were calibrated to convert from pixels to actual dimensions for each combination of filter material, aspect ratio and measurement height (ImageJ 1.37). Coordinates of cylinder locations were recorded and particles for tracking were selected in frame one from those located within in the narrow sector between adjacent

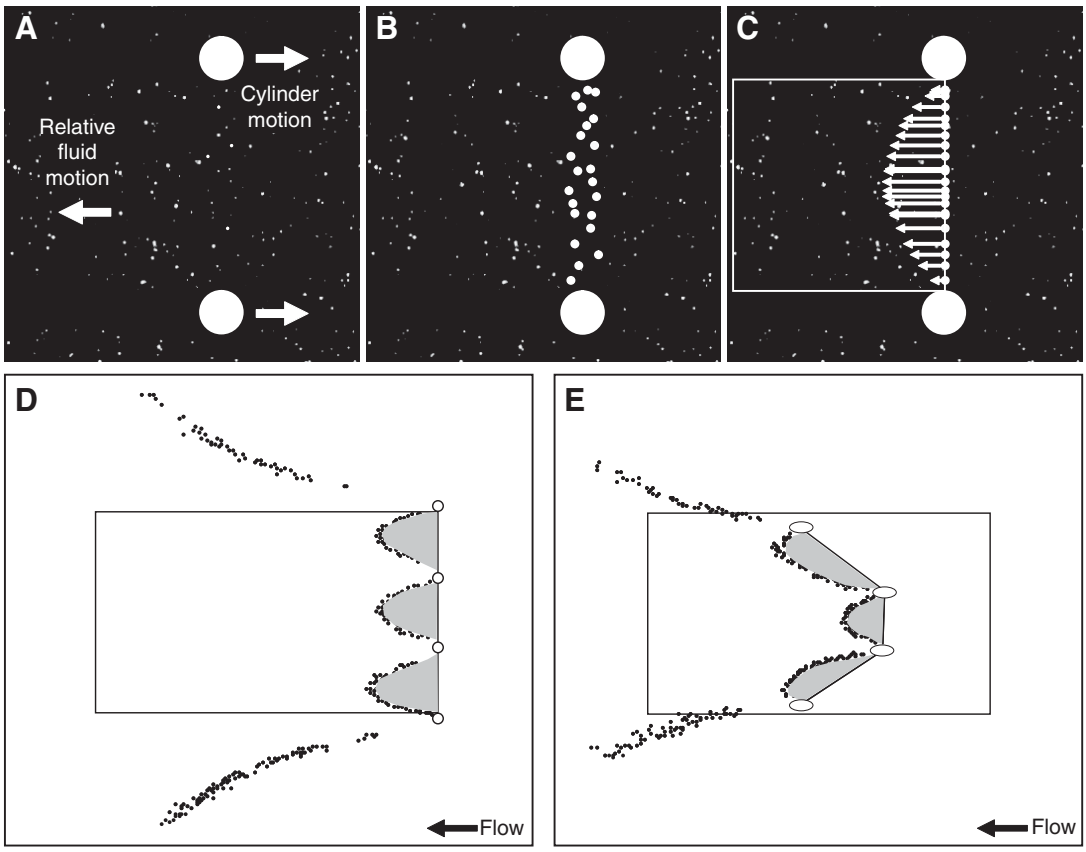

Fig. 2. Overhead view of particle tracking technique used to quantify fluid flow between filter elements (A–C), for calculation of relative flow ('leakiness') through entire filter arrays (D,E). Large white circles indicate cross section of a pair of cylindrical filter elements and small white dots indicate suspended particles used for tracking fluid motion. (A) Filter array and camera were moved from left to right to generate relative fluid motion from right to left. (B) Particles initially positioned between filter elements were used as flow tracers. (C) Particle trajectories resulting from fluid motion were measured and initial positions were adjusted to the centerline between filter elements to determine the mean velocity gradient between elements. The white box represents the total area swept by the pair of filter elements. (D) Composite representation of fluid motion through a rigid filter array (E~177 GPa). Leakiness was calculated by dividing the spatially integrated velocity profile across the width of the array (shaded regions) by the product of undeformed array width and free-stream velocity (bounding box). (E) Composite representation of fluid motion through a flexible filter array (E~1 GPa). Note that the displacement of cylinder cross sections from the right-hand end of the box arose because of streamwise bending that characterized distal regions of the array. Cross-stream narrowing of the array and oblique orientation of bent filter elements are also apparent.

cylinders (Fig. 2). Flow past highly bent cylinders was sometimes deflected vertically, carrying particles out of the imaging plane. To avoid positional ambiguity associated with such vertical movements, only particles that were illuminated through all four frames were tracked and used in estimating velocity. Total horizontal (streamwise) displacement was calculated for each particle and divided by the time interval between the first and fourth frames to obtain particle velocities.

Two distinct leakiness quantities were calculated for each model filter. Estimates of 'planar' leakiness were obtained at each of multiple discrete distances from the filter base by dividing (at each distance) the spatially integrated velocity profile across the width of the array by the product of array width (without deformation) and free-stream velocity. This proportionality equaled the amount of fluid that actually passed through the filter in a plane at a given distance from the base, normalized by the amount of fluid that would have passed through the same space (i.e. the region spanned by the undeformed filter) if the filter were absent. Replicate estimates of planar leakiness were averaged for each filter material and within each combination of velocity and vertical position. Taking each set of planar leakiness values (one value for each of a series of distances from the base of the filter array), the 'whole-model' leakiness was then computed for the entire array in order to account for the proximal-to-distal variation in planar leakiness along the length of the filter. Note that the whole-model leakiness was estimated by averaging the values of planar leakiness across all measurement distances out to L, including those beyond the reduced height of the bent array. This convention effectively normalized the amount of fluid passing through the bent array by the amount of fluid that would, in the absence of the filter, pass through the region spanned by it in its undeflected configuration (as opposed to the amount of fluid that would, in the absence of the filter, pass through the smaller region spanned by it in its bent configuration). Such values of whole-model leakiness thereby captured effects of both decreases in fluid passage through the array and array deformation, when providing an index of overall filter performance.

RESULTS

Fluid and material properties

Syrup density remained nearly constant throughout the study (mean ± s.d.; ρ=1456±27 kg m^{-3}; N=9), but unavoidable changes in room temperature caused modest variation in dynamic viscosity

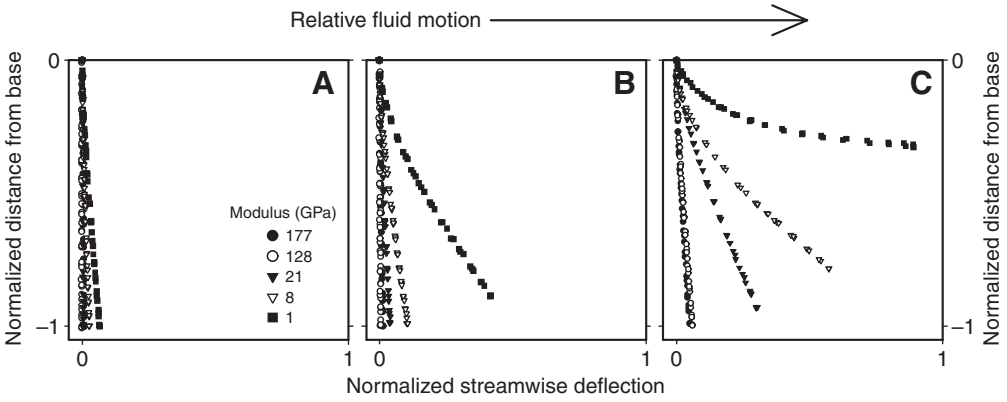

Fig. 3. Side view of deflected filter arrays (*L*/*d*=100) showing that streamwise bending reduced effective filter height to an extent that depended on the elastic modulus of the filter elements. Models were towed at different velocities to produce relative flow at approximate *Re* of (A) 10^{-5}, (B) 10^{-4} and (C) 10^{-3}. Filter elements were anchored in a flat sled at the fluid surface and extended vertically into the fluid when at rest. Plotted positions represent an average of the bending trajectories of inner and outer elements within each array, digitized from photographs (three replicate runs per flow speed). Measured deflections and distances from the filter base were normalized by the height, *L*, of a stationary array. Arrow indicates direction of flow through filters.

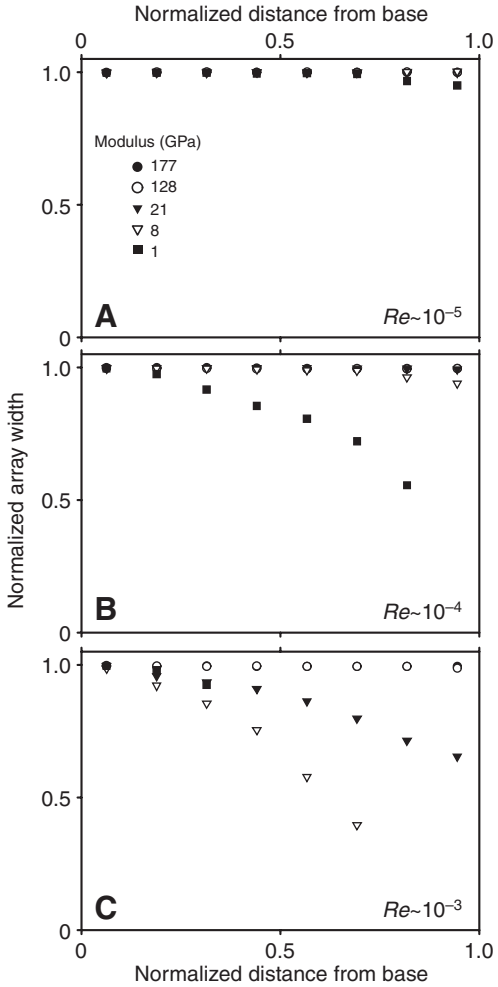

Fig. 4. Cross-stream width of flexible filter arrays (*L*/*d*=100) decreased with distance from the base, illustrating filter narrowing due to flow diversion around the models at approximate *Re* of (A) 10^{-5}, (B) 10^{-4} and (C) 10^{-3}. Measured array widths were normalized by the width of a stationary array and distances from the filter base were normalized by the height, *L*, of a stationary array.

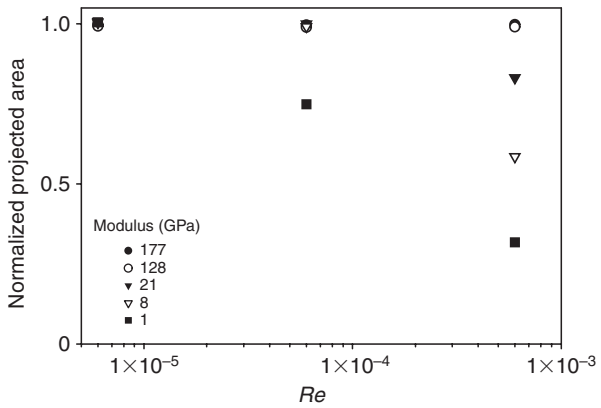

Fig. 5. Projected area of filter arrays (*L*/*d*=100) as a function of *Re*. Decreased filter area at higher *Re* was due to a combination of streamwise bending and cross-stream narrowing of flexible arrays. Measured areas were normalized by the area of a stationary array.

[μ=118±19 N s m^{-2} (*N*=13) for trials with arrays of slender filter elements (*L*/*d*=100); μ=161±5 N s m^{-2} (*N*=10) for trials with arrays of stout filter elements (*L*/*d*=50)]. These conditions resulted in average *Re* values of 5.1×10^{-6}, 5.1×10^{-5} and 5.1×10^{-4}, although for simplicity's sake these experimental conditions are referenced using order-of-magnitude designations (i.e. *Re* of 10^{-5}, 10^{-4} and 10^{-3}). The elastic moduli of the cylinder materials (mean ± s.d.; *N*=4 of each material) spanned a more than 100-fold range in stiffness (stainless steel, 176.50±1.97 GPa; brass, 127.61±0.14 GPa; Garolite-G10, 21.03±1.25 GPa; Garolite-XX, 8.00±0.07 GPa; nylon, 1.37±0.05 GPa) and yielded average *B* values of 1.0×10^{9} to 1.4×10^{15} across conditions.

Filter deformation

Although Eqns 1–3 dictate that flow patterns in our experiments vary formally with *Re*, *L*/*d* and *B* (recall that we held *x*/*d* constant), the parameter *B* includes components associated with both organism material properties (*E*) and free-stream (=tow) velocity (*U*). These two variables can be confusing to manipulate mentally at the same time, which led us to depict filtration

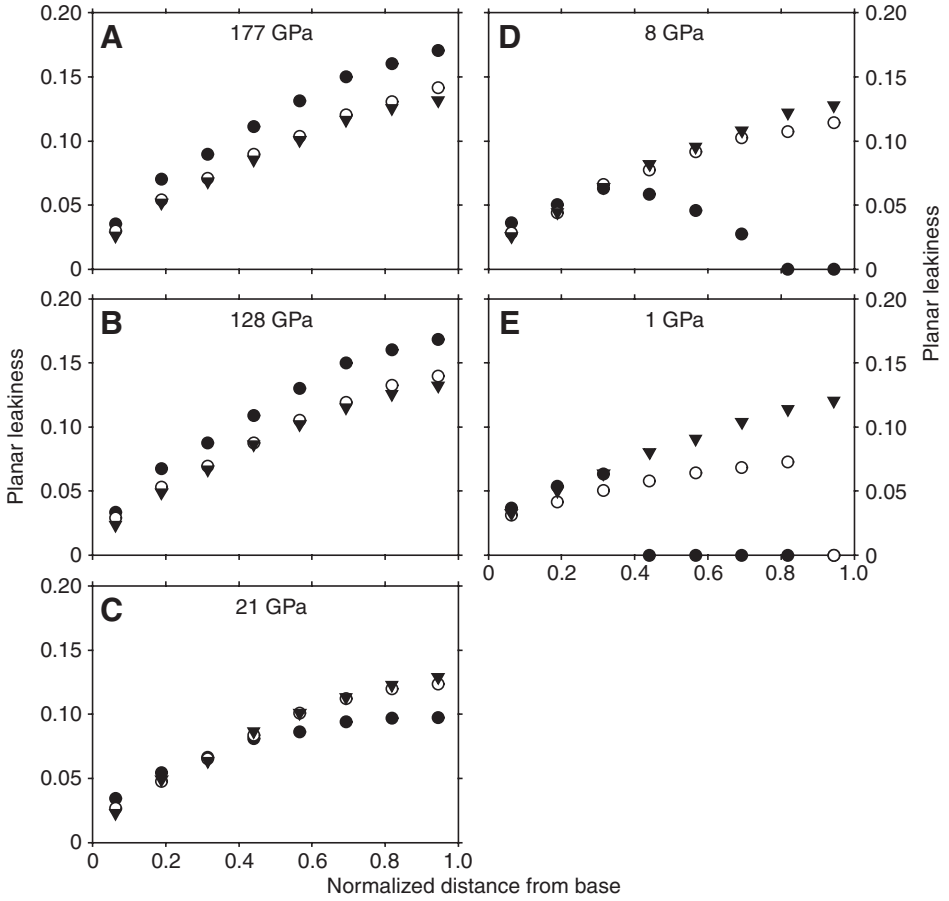

Fig. 6. Planar leakiness of slender-element filter arrays (*L*/*d*=100) *versus* distance from their base at approximate *Re* of 10^{-3} (solid circles), 10^{-4} (open circles) and 10^{-5} (solid triangles). Data for filters of different materials are presented in order of increasing flexibility from A to E. Instances where planar leakiness equals zero indicate severe bending of the filter array that prevented filtration at that height. Distances from the filter base were normalized by the height, *L*, of a stationary array.

consequences of flexibility as a function of absolute stiffness (*E*) instead of normalized stiffness (although values of *B* are available by straightforward substitution). The resultant data demonstrated that model filter arrays of a given modulus exhibited greater bending as tow velocities increased (Fig. 3). Over the range of flow conditions tested, the tip angle of deflection [=arctan(δ/*L*)] of the cylinders averaged across all four filter elements in an array varied from 0.1 to 2.9 deg. for the most rigid material (*E*~177 GPa), and from 3.7 to 70.4 deg. for the most flexible material (*E*~1 GPa). This streamwise bending decreased vertical filter height, as viewed from upstream, by as much as 0.5%, 1.1%, 7.1%, 21.8% or 68.2%, for filters ranging from least to most flexible. The oblique orientation of deflected filter elements also changed the cross-sectional shape of elements penetrating a given horizontal plane (e.g. Fig. 2E), increasing the amount of element surface bordering the planar flow. The two outer filter elements bent farther than the inner elements, probably because the outer elements experienced faster relative velocities and thus higher drag (e.g. Fig. 2E). The latter differential bending was detectable in many of the filter materials and flow conditions but was maximal in the flexible arrays exposed to higher-velocity flows.

Array width also decreased as a function of *Re*, distance from the base of the filter (Fig. 4), and as values of elastic modulus declined. This cross-stream narrowing of an array was expressed through changes in gap width between individual elements and a corresponding increase in the proportion of projected area occluded by the elements themselves. In one case, the outer two filter elements bent inward enough to make contact with the central two elements, thereby minimizing flow through the outer gaps of the array in the region of contact (Fig. 4C; *E*~8 GPa, distance from the filter base=0.7 *L*).

The two effects outlined above, streamwise bending and cross-stream narrowing, together caused a substantial decrease in total projected filter area (Fig. 5). Relative to stationary arrays, filter deformation reduced projected area by as much as 1.0, 4.0, 20.7, 46.0 or 72.1%, for models ranging from least to most flexible. Filter area was similar among arrays composed of all five materials when flow velocities and *Re* were lowest. In the intermediate *Re* condition, only the most flexible array (*E*~1 GPa) deformed appreciably, and in the highest *Re* condition the observed reductions in filter area were inversely correlated with material stiffness. For the most flexible array (*E*~1 GPa) in the highest *Re* condition, streamwise bending dominated the reduction in projected area because extreme bending restricted the vertical filter span to only three measurement distances from the base (e.g. Fig. 3C; Fig. 4C).

Planar leakiness

Planar leakiness averaged across the width (three gaps) of each array varied systematically with distance from the array base, *Re*, and elastic modulus (Fig. 6). Maximum planar leakiness associated with any of the test conditions was only 0.17 because of pronounced velocity retardation in the boundary layer over the sled and substantial flow diversion around the filter arrays, as would be expected for low *Re* conditions. All filters exhibited comparable leakiness for planes immediately beneath the sled where the local angle of cylinder deflection was negligible. The general increase in leakiness with distance from the array base was attributed to the

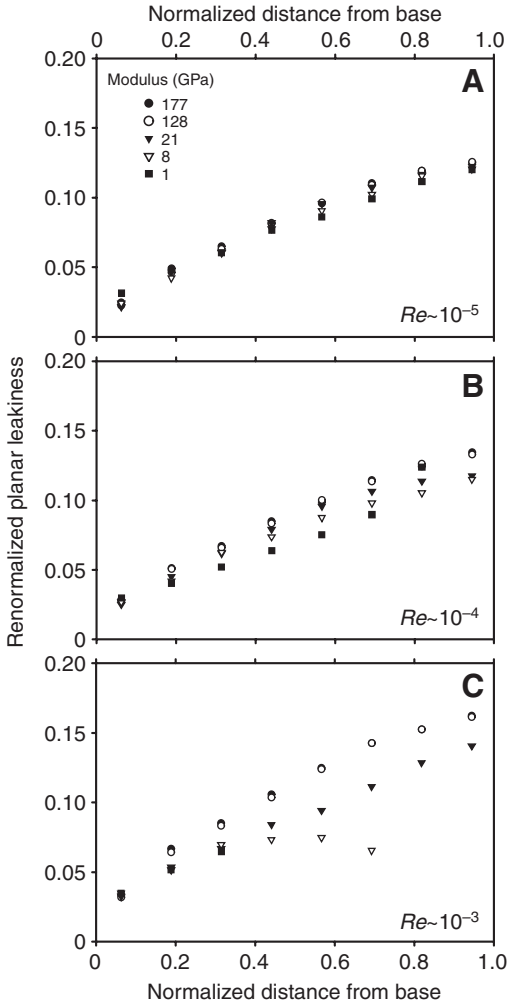

Fig. 7. Renormalized planar leakiness (i.e. calculated relative to instantaneous rather than idealized array width) *versus* distance from the base of filter arrays (*L*/*d*=100) operating at approximate *Re* of (A) 10^{-5}, (B) 10^{-4}, and (C) 10^{-3}. Divergent trajectories evident in B and C illustrate changes in leakiness that were independent of variation in array width. Distances from the filter base were normalized by the height, *L*, of a stationary array.

velocity gradient established over the sled, which led to faster relative flow speeds in planes farther from the sled.

For the most rigid filter arrays (*E*~128, 177 GPa), filter leakiness was dependent on current speed, with the greatest leakiness occurring in the highest *Re* flow (Fig. 6A,B). This positive trend in planar leakiness with increasing *Re* was reversed for filters composed of the other three materials (*E*~1, 8, 21). In these more flexible arrays, leakiness was reduced in fast flows. This reversal was most apparent in the highest *Re* condition where strong streamwise bending prevented filtration far from the filter base in the two most flexible arrays (*E*~1, 8), producing leakiness values that were effectively zero for the most distal measurement planes (Fig. 6D,E).

Further examination of planar leakiness revealed a subtler effect of cylinder bending that was independent of changes in filter area. For any given filter array and distance from the filter base, one might expect that variations in planar leakiness would correspond to variations in array width. This expectation held for model filters that experienced relatively little deflection, but when streamwise bending was more pronounced, observed reductions in planar leakiness were modified. We evaluated this trend by calculating a 'renormalized' value of planar leakiness that controlled for the influence of changing array width. For every combination of filter material, tow velocity and distance from the base, values of renormalized planar leakiness were obtained by dividing the spatially integrated velocity profile across the width of the array by the product of narrowed array width (i.e. accounting for deformation) and free-stream velocity. The resultant estimates of renormalized planar leakiness were then plotted as a function of distance from the array base for all filter materials and *Re* conditions (Fig. 7). If changes in array width alone had accounted for the previously observed reductions in planar leakiness through more flexible filters (Fig. 6), then renormalized planar leakiness values should have been identical for all filters operating at a given *Re*, regardless of their material stiffness. This default outcome, however, did not occur. Instead, additional reductions in water flow between filter elements arose in association with the oblique orientation of deflected elements, probably as a result of the combination of vertical diversion of flow around a bent filter array (resulting in lower horizontal velocities impinging on the filter) and increased resistance to flow through the filter due to more element surface bordering each gap (cf. elliptical cross sections in Fig. 2E).

Effects of element flexibility on renormalized planar leakiness also appeared to intensify with increasing *Re* and filter deflection (Fig. 7B,C). However, careful inspection revealed an experimental artifact associated with extreme levels of element bending due to our method of flow visualization. Beyond a certain distance from the filter base, the substantial reductions in renormalized planar leakiness associated with filter deformation became relatively less pronounced. This shift can be explained by the observation that bent cylinders within an array did not stabilize at precisely the same height. Particularly at large distances from the base of a flexible array, bending of the outer elements exceeded that of the inner ones (e.g. Fig. 2E) and resulted in vertical separation of elements that caused the absolute distance between adjacent elements to become greater than the observed (horizontal) separation when looking straight down on the filter array. This vertical separation of filter elements changed the three-dimensional flow patterns such that measured fluid motion through the 'observed gap' became greater than expected.

Effects of aspect ratio

Additional tests using arrays of shorter and proportionally thicker (stouter) filter elements (*L*/*d*=50) of the same materials showed a similar but less pronounced pattern than the slender arrays (Fig. 8). Maximum planar leakiness (through the most rigid filters) was 0.13, representing a 14% reduction from the maximum leakiness through the slender arrays. Planar leakiness near the base was similar among model filters (~0.03) but the increase in leakiness with distance from the base was suppressed by filter deformation, although this effect was weaker than that observed for the slender arrays. Relative to average maximum leakiness through the rigid filters, leakiness at the most distal measurement plane decreased by 16% and 11% for stout arrays in which *E*~8 and 21 GPa, respectively, representing a milder consequence of bending than was observed in slender arrays (e.g. Fig. 6C,D). In the highest *Re*, the most flexible stout array (*E*~1 GPa) deformed enough to prevent filtration far from the filter base, consequently reducing leakiness relative to the lower *Re* conditions (Fig. 8E), but again this reduction in leakiness was far

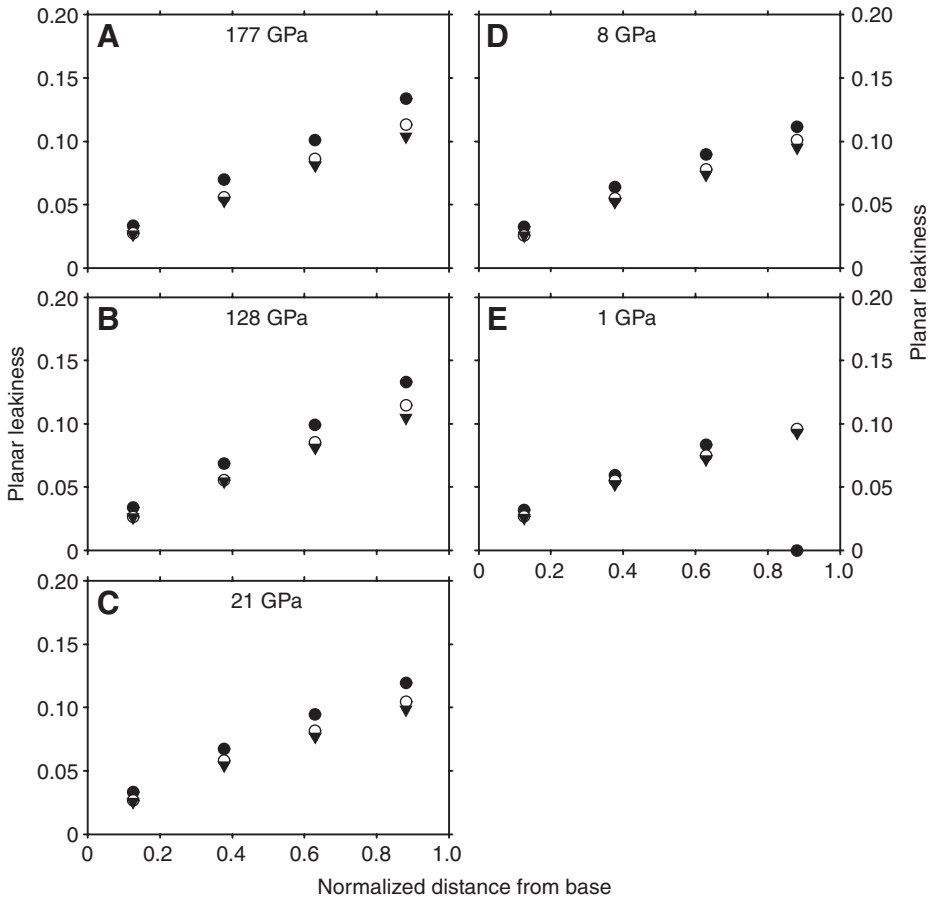

Fig. 8. Planar leakiness of stout-element filter arrays (L/d=50) *versus* distance from the base at approximate *Re* of 10^{-3} (solid circles), 10^{-4} (open circles) and 10^{-5} (solid triangles). Data for filters of different materials are presented in order of increasing flexibility from A to E. The case where planar leakiness equaled zero in E indicates severe bending of the filter array that prevented filtration at that height. Distances from the filter base were normalized by the height, *L*, of a stationary array.

less than that in slender arrays where more than 50% of the filter span was effectively eliminated by bending (Fig. 6E).

Whole-model leakiness

Whole-model leakiness, computed by integrating planar leakiness across the full height of the filter array (Fig. 9), illustrated the overall effect of structural flexibility for filter function. One critical trend was the different behavior of rigid *versus* flexible filters, especially for the slender arrays. In general, whole-model leakiness of rigid filters (E~128, 177) increased with *Re*. In our study, average whole-model leakiness through the most rigid arrays of slender elements (L/d=100) increased by 24% between *Re* of 10^{-4} and 10^{-3}, compared to an increase of only 5% between *Re* of 10^{-5} and 10^{-4} (Fig. 9A). In marked contrast, the three more flexible arrays exhibited the opposite trend in whole-model leakiness. For instance, the most flexible slender array (E~1) exhibited a dramatic, 41% decline in leakiness between *Re* of 10^{-5} and 10^{-4} and an additional decrease of 60% between *Re* of 10^{-4} and 10^{-3}. The effect was similar, although somewhat muted, in the second most flexible (E~8) and intermediately flexible (E~21) arrays. These filter arrays experienced decreases in leakiness of 55% and 10%, respectively, between the intermediate and high *Re* conditions. The most pronounced reductions in leakiness resulted primarily from effective shortening of the filters, which led to zero filtration at fixed distances far from the filter base in the two most flexible arrays (Fig. 6D,E).

A similar, but less dramatic pattern also arose in filters composed of stouter elements (L/d=50; Fig. 9B). Whole-model leakiness of the most flexible stout array showed a 28% decrease across the range of *Re* conditions examined. Importantly, even though flexibility-induced reductions in leakiness with increased *Re* were smaller in stout arrays as compared to slender arrays, stout arrays still often processed less fluid (i.e. had lower overall leakiness). This trend reflects the commonly (but not universally) poorer filtering abilities of stout arrays, most apparent at larger *Re* in the rigid-element data. For instance, average whole-model leakiness of the two most rigid filters (E~128, 177) in the highest *Re* condition was 0.08 for stout arrays *versus* almost 0.12 for slender arrays. Given that cylinder diameters, gap widths, array width, and fraction of projected area occluded by filter elements were equivalent among the most rigid filter arrays, observed reductions in leakiness through the stout arrays can be fully attributed to their lower position in the boundary layer formed over the tow sled.

DISCUSSION

General trends

Results indicate that flexible filter arrays process less water than more rigid arrays (Fig. 9). This decrease in leakiness derives from changes to projected filter area (Figs 3–5) and reduced flow through deflected arrays (Fig. 7). The reduction in filter area is due to both streamwise bending and cross-stream narrowing, but the influence of bending dominates under conditions of extreme deflection. Structural deformation also reduces the degree to which the filter extends through the boundary layer and it leads to slower velocities impinging on the filter.

Patterns of whole-model (integrated) leakiness also demonstrate that filter flexibility can alter the relationship between filter leakiness and *Re*, particularly in arrays composed of slender elements. Prior

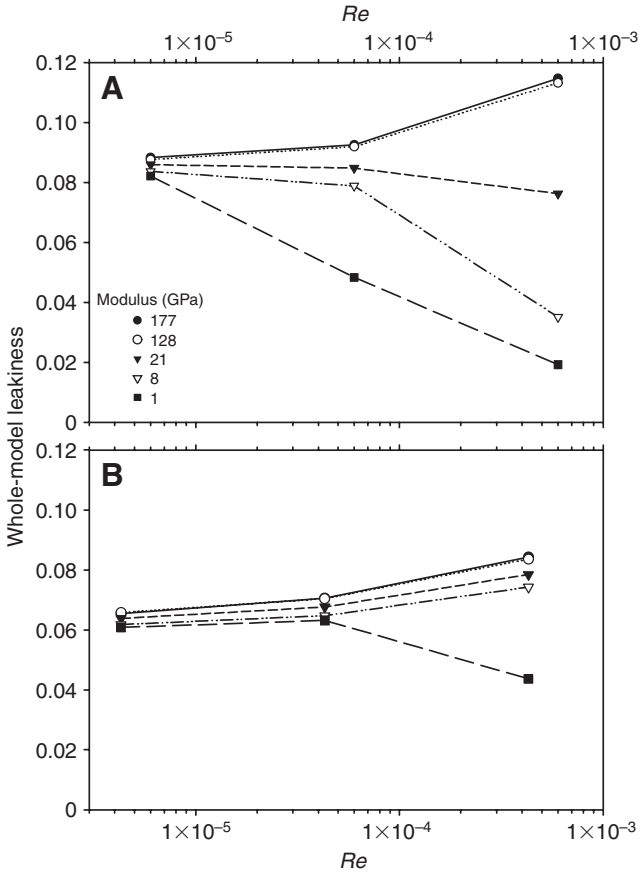

Fig. 9. Whole-model leakiness *versus Re* for arrays of filter elements having an aspect ratio of (A) L/d=100 and (B) L/d=50. The diverging pattern in A illustrates the susceptibility of slender-element arrays to flexibility-related reductions in leakiness, an effect that became more pronounced in faster flows. Consequences of structural flexibility were reduced in stout-element arrays (B), but a diverging pattern was still apparent in the highest *Re* condition.

studies of leakiness through rigid filter arrays have found that leakiness increases gradually over *Re* from 10^{-5} to 10^{-3}, in contrast to filters operating at slightly higher *Re* where leakiness is very sensitive to *Re* (Cheer and Koehl, 1987; Koehl, 1995). However, data presented here suggest that deformation of feeding appendages may incur a cost of reduced leakiness across a range of low *Re*, potentially altering expectations of when critical transitions in filter function may occur. Our results also suggest the need to re-evaluate the notion that slender (as opposed to stout) elements in filter arrays always ensure greater leakiness, given that this trend may disappear in the presence of substantial deformation (compare case for E~1 GPa at the highest *Re* condition in Fig. 9A,B). Such neglected aspects of filter function may require some adjustment to existing perceptions regarding linkages between morphology and ecology in suspension feeders.

Experimental considerations

Although strong trends are apparent in the results above, some care should also be applied in their interpretation. Findings are relevant to low-*Re* conditions representative of suspension feeders on the small end of the size spectrum, and quantitative values underlying the overall qualitative patterns may apply rigorously only to specific geometries. Examples of organisms that operate at $Re \sim 10^{-5}$ whose filter structures resemble those studied here include nanoplanktonic flagellates (e.g. *Actinomonas mirabilis*; L/d ~60; $\boldsymbol{g}/d$ ~5; x/d ~20) (Fenchel, 1982). Suspension feeders that function at $Re \sim 10^{-4}$ include cladocerans (e.g. *Penilia avirostris*, with L/d ~45; $\boldsymbol{g}/d$ ~6; x/d ~15) (Turner et al., 1988). There are many organisms that feed at $Re \sim 10^{-3}$ and use filters analogous in shape to those of this study (e.g. *Euphausia superba*, with L/d ~ 60; $\boldsymbol{g}/d$ ~4; x/d ~10) (McClatchie and Boyd, 1983).

Complete effects of reduced filter area also may not be evident in our analysis because flow was measured though a finite number of horizontal planes. We were therefore forced to assume that leakiness through interior portions of arrays where flow was not quantified (i.e. regions between measurement heights) could be reasonably approximated by interpolation. However, contributions to leakiness from the extreme upper, and sometimes lower, portions of each filter were not represented. Material imperfections in individual filter elements also may have contributed to variability in the leakiness calculations, as they occasionally caused slight non-uniformities in bending. These inconsistencies likely resulted from asymmetries introduced during manufacture of the model elements, although analogous effects could also play a role in the bending trajectories of actual animal feeding appendages. We further note that although observations of invertebrate suspension feeders reveal that bending of their particle capture apparatus is common, quantitative evaluations of the moduli of these structures are generally unavailable. For our purposes, we assumed that the stiffnesses of suspension-feeding structures are similar to those of the 'building-block' materials from which they are composed, and for which there are data. For example, skeletal components such as chitin and keratin have elastic moduli of 1–100 GPa, and structures reinforced with calcium carbonate have elastic moduli less than 100 GPa (Wegst and Ashby, 2004). Assuming stiffnesses across this range, the materials we employed in our experiments corresponded to biologically relevant ranges of nondimensional stiffness (B). However, it is also possible that some suspension feeders produce particle capture apparatuses that diverge from values of B used in our experiments.

Filters in the natural environment

Leakiness patterns presented here reveal new insights into the function of filters operating in steady flows at very low *Re* (e.g. in pelagic environments or in tidal currents where changes occur over timescales of hours). Our findings may be less applicable to flows associated with rapidly evolving waves or turbulence, such as those found in intertidal or shallow subtidal habitats (Gaylord, 1999; Gaylord, 2000; Gaylord, 2008). In these latter environments, filter deformation and its implications for particle capture could be either suppressed or intensified depending on the combined effect of fluid reversals and vortex attachment or shedding. During periods of accelerating or decelerating flow, for example, the bending trajectories of even moderately flexible filters might lag behind flow reversals and thus damp fluctuations in relative velocities. Some microhabitats where benthic suspension feeders settle will also experience velocity bursts as the effects of turbulent eddies penetrate all the way to the seafloor (Cantwell, 1981; Dade, 1993). Individuals living in topographical microhabitats where velocity transients are common could experience disproportionate consequences of filter deflection. We also note that the bending of biological filters may influence the function of array-like structures in organisms beyond marine suspension feeders. Low-*Re* filters are employed for respiration, propulsion and olfaction in a wide variety of freshwater and terrestrial invertebrates (see e.g. Loudon and Koehl, 2000; Sunada et al., 2002; Barta and Weihs, 2006). Deformation-induced

effects on leakiness probably play paramount roles in these organisms as well.

Conclusions

Our results concern leakiness, and not particle encounter or capture (e.g. Palmer et al., 2004), and therefore do not address the full suite of factors driving food acquisition by mechanisms of hydrosol filtration. However, fluid transmission through a filter array is one of the fundamental gatekeepers for particle capture. Here, we show that structural flexibility can compromise leakiness across a range of low *Re* conditions. Detrimental effects of filter deformation on leakiness generally increase with *Re* and are offset in some cases for stouter filter elements. Such consequences of material properties and element shape for filter leakiness are likely to have important implications for suspension feeders of a variety of morphologies. Future studies should examine effects of flexibility across a greater spectrum of filter geometries and at higher *Re*, and should examine other steps in the feeding process (encounter and retention). Such work will facilitate the development of more comprehensive predictions of how food acquisition varies with collector morphology, flow conditions, and particle size and concentration.

LIST OF SYMBOLS

B	nondimensional stiffness
d	element diameter (m)
δ	element tip deflection (m)
E	elastic modulus ($N\,m^{-2}$)
F	force (N)
L	element length (m)
Re	Reynolds number
U	velocity ($m\,s^{-1}$)
x	distance from leading edge (m)
μ	dynamic viscosity ($Ns\,m^{-2}$)
ρ	density ($kg\,m^{-3}$)

We are grateful to P. Jumars and an anonymous reviewer for feedback on previous versions of the paper. M. Petty assisted with design and construction of the low Reynolds number tank and tow sled, and enthusiastically helped produce the thinnest possible light sheet. This research was funded by NSF grants OCE-021447 and OCE-0523870, and the University of California Marine Council Coastal Environmental Quality Initiative grant 04-T-CEQI-08-0048. Contribution 2432 Bodega Marine Laboratory, University of California at Davis.

REFERENCES

Barta, E. and Weihs, D. (2006). Creeping flow around a finite row of slender bodies in close proximity. *J. Fluid Mech.* **551**, 1-17.
Cantwell, B. J. (1981). Organized motion in turbulent flow. *Annu. Rev. Fluid Mech.* **13**, 457-515.
Cheer, A. Y. L. and Koehl, M. A. R. (1987). Paddles and rakes: fluid flow through bristled appendages of small organisms. *J. Theor. Biol.* **129**, 17-39.
Dade, W. B. (1993). Near-bed turbulence and hydrodynamic control of diffusional mass-transfer at the sea-floor. *Limnol. Oceanogr.* **38**, 52-69.
Eckman, J. E. and Nowell, A. R. M. (1984). Boundary skin friction and sediment transport about an animal-tube mimic. *Sedimentology* **31**, 851-862.
Fenchel, T. (1982). Ecology of heterotrophic microflagellates. I. some important forms and their functional morphology. *Mar. Ecol. Prog. Ser.* **8**, 211-223.
Fox, R. W. and McDonald, A. T. (1985). *Introduction to Fluid Dynamics*, 3rd edn. New York: John Wiley and Sons.
Gaylord, B. (1999). Detailing agents of physical disturbance: wave-induced velocities and accelerations on a rocky shore. *J. Exp. Mar. Biol. Ecol.* **239**, 85-124.
Gaylord, B. (2000). Biological implications of surf-zone complexity. *Limnol. Oceanogr.* **45**, 174-188.
Gaylord, B. (2008). Hydrodynamic context for considering turbulence impacts on external fertilization. *Biol. Bull.* **214**, 315-318.
Gili, J. M. and Coma, R. (1998). Benthic suspension feeders: their paramount role in littoral marine food webs. *Trends Ecol. Evol.* **13**, 316-321.
Hansen, B. and Tiselius, P. (1992). Flow through the feeding structures of suspension feeding zooplankton: a physical model approach. *J. Plant. Res.* **14**, 821-834.
Harvell, C. D. and LaBarbera, M. (1985). Flexibility: a mechanism for control of local velocities in hydroid colonies. *Biol. Bull.* **168**, 312-320.
Hunter, T. (1989). Suspension feeding in oscillatory flow: the effect of colony morphology and flow regime on plankton capture by the hydroid *Obelia longissima*. *Biol. Bull.* **176**, 41-49.
Koehl, M. A. R. (1995). Fluid flow through hair-bearing appendages: feeding, smelling and swimming at low and intermediate Reynolds numbers. In *Biological Fluid Dynamics* (ed. C. P. Ellington and T. J. Pedley), pp. 157-182. Cambridge: Company of Biologists.
Koehl, M. A. R. and Strickler, J. R. (1981). Copepod feeding currents: food capture at low Reynolds number. *Limnol. Oceanogr.* **26**, 1062-1073.
LaBarbera, M. (1984). Feeding currents and particle capture mechanisms in suspension feeding animals. *Am. Zool.* **24**, 71-84.
Lacoursière, J. O. and Craig, D. A. (1993). Fluid transmission and filtration efficiency of the labral fans of black fly larvae (Diptera: Simuliidae): hydrodynamic, morphological, and behavioural aspects. *Can. J. Zool.* **71**, 148-162.
Larsson, A. I. and Jonsson, P. R. (2006). Barnacle larvae actively select flow environments supporting post-settlement growth and survival. *Ecology* **87**, 1960-1966.
Leonard, A. B. P. (1992). The biomechanics, autoecology and behavior of suspension-feeding in crinoid echinoderms. PhD Thesis, University of California, San Diego, CA, USA.
Leonard, A. B., Strickler, J. R. and Holland, N. D. (1988). Effects of current speed on filtration during suspension feeding in *Oligometra serripinna* (Echinodermata: Crinoidea). *Mar. Biol.* **97**, 111-125.
Loudon, C., Best, B. A. and Koehl, M. A. R. (1994). When does motion relative to neighboring surfaces alter the flow through arrays of hairs? *J. Exp. Biol.* **193**, 233-254.
Loudon, C. and Koehl, M. A. R. (2000). Sniffing by a silkworm moth: wing fanning enhances air penetration through and pheromone interception by antennae. *J. Exp. Biol.* **203**, 2977-2990.
McClatchie, S. and Boyd, C. M. (1983). Morphological study of sieve efficiencies and mandibular surfaces in the Antarctic krill, *Euphausia superba*. *Can. J. Fish. Aquat. Sci.* **40**, 955-967.
Mead, K. S. and Koehl, M. A. R. (2000). Stomatopod antennule design: the asymmetry, sampling efficiency and ontogeny of olfactory flicking. *J. Exp. Biol.* **203**, 3795-3808.
Palmer, M. R., Nepf, H. M. and Pettersson, T. J. R. (2004). Observations of particle capture on a cylindrical collector: implications for particle accumulation and removal in aquatic systems. *Limnol. Oceanogr.* **49**, 76-85.
Patterson, M. R. (1984). Patterns of whole colony prey capture in the octocoral, *Alcyonium siderium*. *Biol. Bull.* **167**, 613-629.
Patterson, M. R. (1991). The effects of flow on polyp-level prey capture in an octocoral, *Alcyonium siderium*. *Biol. Bull.* **180**, 93-102.
Rubenstein, D. I. and Koehl, M. A. R. (1977). The mechanisms of filter feeding: some theoretical considerations. *Am. Nat.* **111**, 981-994.
Scardino, A. J., Guenther, J. and de Nys, R. (2008). Attachment point theory revisited: the fouling response to a microtextured matrix. *Biofouling* **24**, 45-53.
Schlichting, H. (1979). *Boundary-Layer Theory*, 7th edn. New York: McGraw-Hill.
Shimeta, J. and Jumars, P. A. (1991). Physical mechanisms and rates of particle capture by suspension-feeders. *Oceanogr. Mar. Biol. Annu. Rev.* **29**, 191-257.
Sponaugle, S. and LaBarbera, M. (1991). Drag-induced deformation: a functional feeding strategy in two species of gorgonians. *J. Exp. Mar. Biol. Ecol.* **148**, 121-143.
Sunada, S., Takashima, H., Hattori, T., Yasuda, K. and Kawachi, K. (2002). Fluid-dynamic characteristics of a bristled wing. *J. Exp. Biol.* **205**, 2737-2744.
Turner, J. T., Tester, P. A. and Ferguson, R. L. (1988). The marine cladoceran *Penilia avirostris* and the "microbial loop" of pelagic food webs. *Limnol. Oceanogr.* **33**, 245-255.
Vogel, S. (1994). *Life in Moving Fluids: The Physical Biology of Flow*. Princeton: Princeton University Press.
Wegst, U. G. K. and Ashby, M. F. (2004). The mechanical efficiency of natural materials. *Philos. Mag.* **84**, 2167-2181.
Wildish, D. and Kristmanson, D. (1997). *Benthic Suspension Feeders and Flow*. New York: Cambridge University Press.